Road Boundary Detection using In-vehicle Monocular Camera

Kazuki Goro and Kazunori Onoguchi
Graduate School of Science and Technology, Hirosaki University, 3 Bunkyo-cho, Hirosaki, 036-8561, Japan

Keywords: Inverse Perspective Mapping, ITS, Shoulder of a Road, Snow Wall, Snakes.

Abstract: When a lane marker such as a white line is not drawn on the road or it's hidden by snow, it's important for the lateral motion control of the vehicle to detect the boundary line between the road and the roadside object such as curbs, grasses, side walls and so on. Especially, when the road is covered with snow, it's necessary to detect the boundary between the snow side wall and the road because other roadside objects are occluded by snow. In this paper, we proposes the novel method to detect the shoulder line of a road including the boundary with the snow side wall from an image of an in-vehicle monocular camera. Vertical lines on an object whose height is different from a road surface are projected onto slanting lines when an input image is mapped to a road surface by the inverse perspective mapping. The proposed method detects a road boundary using this characteristic. In order to cope with the snow surface where various textures appear, we introduce the degree of road boundary that responds strongly at the boundary with the area where slant edges are dense. Since the shape of the snow wall is complicated, the boundary line is extracted by the Snakes using the degree of road boundary as image forces. Experimental results using the KITTI dataset and our own dataset including snow road show the effectiveness of the proposed method.

1 INTRODUCTION

For the past several decades, many vision-based lane detection methods have been proposed for advanced driver assistance system or autonomous driving system(M. Bertozzi, A. Broggi, M. Cellario, A. Fascioli, P. Lombardi and M. Porta, 2002)(J. C. McCall and M. M. Trivedi, 2006)(B. Hillel, R. Lerner, D. Levi, and G. Raz, 2014). Most of these methods detect lane markers such as white lines from an image and estimate a traffic lane. In the literature (M. Bertozzi and A. Broggi, 1998), a belt-like region whose width is constant and whose brightness is higher than a road surface is detected as a lane marker. In the literature (J.Douret, R. Labayrade, J. Laneurit and R. Chapuis, 2005), a lane marker is detected from a pair of the positive edge and the negative edge with constant distance. The literature (M. Meuter, S. Muller-Schneiders, A. Mika, S. Hold, C. Numm and A. Kummert, 2009) proposes the method that detects a boundary of the white line from a peak of the histogram of edge gradient. The literature (C. Kreucher and S. Lakshmanan, 1999) proposes the method that detects a lane marker by extracting a slanting edge by DCT. The method to detect a broken line(S. Hold, S. Gormer, A. Kummert, M. Meuter, S. Muller-Schneiders, 2010) or a zebra line(G. Thomas, N. Jerome and S. Laurent, 2010) by a frequency analysis is also proposed. The literature (Z. W. Kim, 2008) detects a lane marker by a discriminator created by learning many lane marker images.

Although these methods are effective for roads on which lane markers are drawn, they can not be applied to roads without lane markers or roads covered with snow. In these cases, it's necessary to detect the boundary line between the road and the roadside object such as curbs (Fig. 1(a)), grasses (Fig. 1(b)),side walls (Fig. 1(c)) and so on, instead of lane markers. Especially, when the road is covered with snow, the boundary with the snow side wall (Fig. 1(d)(e)(f)) needs to be detected since other roadside objects are hidden by snow.

To detect a shoulder of the road, several methods using color (M. A. Turk, D. G. Morgenthaler, K. D. Gremban and M. Marra, 1988) and texture(J. Zhang and H. Nagel, 1994) have been proposed. However, when a road is covered with snow, it's difficult to detect a road boundary by color and texture because there are various kinds of snow surfaces, such as the rough snow surface (Fig. 1(d)), the rutted snow surface (Fig. 1(e)), and smooth white snow surface (Fig. 1(f)).

Since road shoulder is usually different in height from a road plane, many methods using depth infor-

Goro, K. and Onoguchi, K.
Road Boundary Detection using In-vehicle Monocular Camera.
DOI: 10.5220/0006589703790387
In *Proceedings of the 7th International Conference on Pattern Recognition Applications and Methods (ICPRAM 2018)*, pages 379-387
ISBN: 978-989-758-276-9

mation obtained by a stereo camera have been proposed(D. Pfeiffer and U. Franke, 2010)(N. Einecke and J. Eggert, 2013)(J. K. Suhr and H. G. Jung, 2013)(C. Guo, J. Meguro, Y. Kojima and T. Naito, 2013)(M. Enzweiler, P. Greiner, C. Knoppel and U. Franke, 2013)(J. Siegemund, D. Pfeiffer, U. Franke and W. Forstner, 2010). However, a stereo camera is more expensive than a monocular camera and it takes time and effort to install because strict calibration between two cameras is needed.

Road detection method based on semantic segmentation has also been proposed. The literature (J. M. Alvarez, T. Gevers and A. M. Lopez, 2010) proposes the method which extracts road area by combining 3D road cues, such as a horizon line, a vanishing point and road geometry, and temporal road cues in Bayesian framework. The literature (D. Hoiem, A. A. Efros and M. Hebert, 2007) detects road area by describing the 3D scene orientation of each image region coarsely. The literatures (J. M. Alvarez, Y. LeCum, T. Gevers and A. M. Lopez, 2012) and (J. M. Alvarez, T. Gevers, Y. LeCum and A. M. Lopez, 2012) propose the method which detects road area by Convolutional Neural Networks. The literature (D. Levi, N. Garnett and E. Fetaya, 2015) proposed the StixelNet whose input is Stixel instead of images. The literature (C. Brust, S. Sickert, M. Simon, E. Rodner and J. Denzler, 2015) detects road area by Convolutional Patch Network whose input is a single image patch extracted around a pixel to be labelled. In the literatures (R. Mohan, 2014) and (G. L. Oliveira, W. Burgard and T. Brox, 2016), road detection method which combines deep deconvolutional and convolutional neural networks is proposed. The literature (A. Laddha, M. K. Kocamaz , L. E. N-serment, and M. Hebert, 2016) proposes a boosting based method for semantic segmentation of road scenes. The literature (D. Costea and S. Nedevschi, 2017) proposes road detection method which reduces human labeling effort by a map-supervised approach. These methods show considerably good results in various road scenes but the results applied to the snow road are not shown.

This paper proposes the novel method that can detect a road boundary from an image of a monocular camera even if a road is covered with snow. Vertical lines on an object whose height is different from a road surface are projected onto slanting lines when an input image is mapped to a road surface by the inverse perspective transformation. Our method detects a road boundary using this characteristic. We introduce the degree of road boundary whose value increases at the boundary with the area where slanting edges are dense. Road boundary is extracted by the Snakes using the degree of road boundary as image forces.

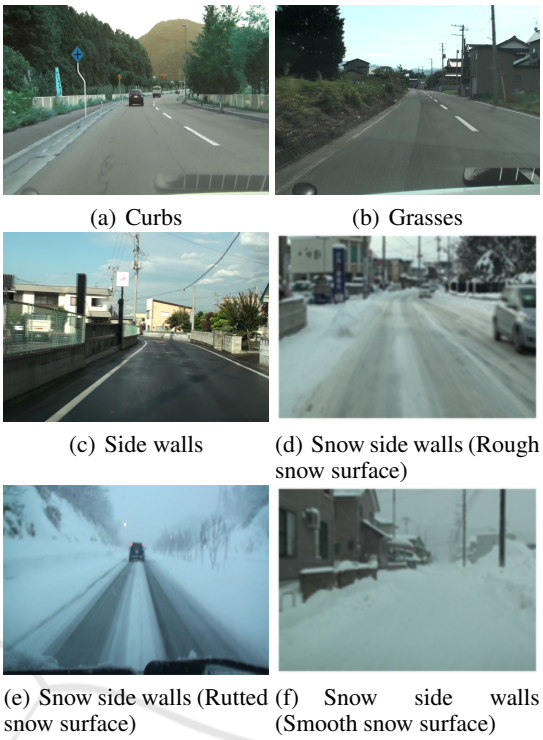

(a) Curbs (b) Grasses

(c) Side walls (d) Snow side walls (Rough snow surface)

(e) Snow side walls (Rutted snow surface) (f) Snow side walls (Smooth snow surface)

Figure 1: Road boundary.

This paper is organized as follows. Section 2 shows the outline of the proposed method. Section 3 explains how to create the Inverse Perspective Mapping (IPM) image from an input image. Section 4 explains the method to create IPM edge image that emphasizes slant edges on road side objects. Section 5 explains the method to calculate the degree of road boundary in each pixel of the IPM edge image. Section 6 describes the method to track the road boundary by the Snakes. Section 7 discusses experimental results performed to several road scenes. Conclusions are presented in Sect. 8.

2 THE OUTLINE OF THE PROPOSED METHOD

Figure 2 shows the procedure of the proposed method. The road boundary is detected in the Inverse Perspective Mapping (IPM) image. In the IPM image, the patterns existing on the road surface are projected to the shape viewed from the right overhead. On the other hand, as shown in Fig. 3, road side objects or obstacles whose height is different from the road surface are projected to the shape falling backward from the location where the obstacles touch the road plane. Therefore, the proposed method detects the boundary

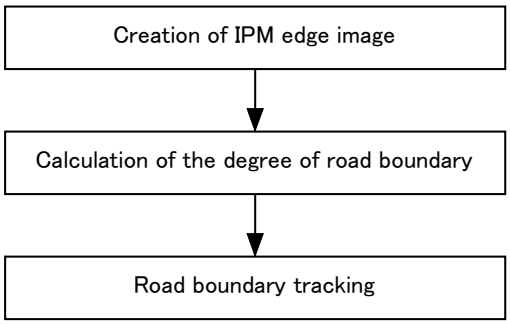

Figure 2: Outline of the proposed method.

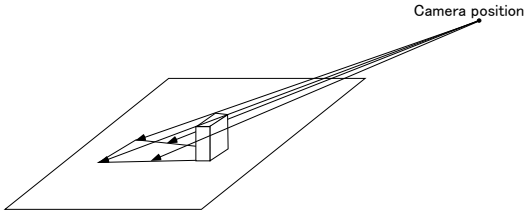

Figure 3: Shape of projected area.

between dense areas of slant edges and sparse areas of slant edges as the road boundary since a lot of slant edges appear around a road side in the IPM image (Fig. 4). First, the IPM edge image that emphasizes slant edges on road side objects is created. Next, the degree of road boundary whose value increases at the boundary with the dense areas of slant edges is calculated in each pixel of the IPM edge image. Finally, the road boundary is tracked by the Snakes whose image force is the degree of road boundary.

3 CREATION OF IPM IMAGE

The inverse perspective mapping (IPM) image, which overlooks a road surface, is created by inverse perspective transform. A point (x,y) in the image coordinate system and a point (u,v) in the IPM image coordinate system satisfy

$$(u,v) = (RX\frac{x-V_{px}}{y-V_{py}}, \frac{RY^2}{y-V_{py}} - \frac{RY^2}{y_{lim}}), \qquad (1)$$

where (V_{px},V_{py}) is the position of a vanishing point in the image coordinate system, RX and RY are compression or expansion rates for direction x and y, and y_{lim} is the lower limit of y-coordinate value in the image(T. Yasuda and K. Onoguchi, 2012). Figure 5(b) shows the IPM image created from Fig. 5(a). Parameters (V_{px},V_{py}), RX, RY and ylim are calibrated when the camera is installed in the vehicle. Unless the camera position changes, these parameter are fixed. In experiments, the IPM image whose size is 640×480 is created from an input image whose size is 640×480.

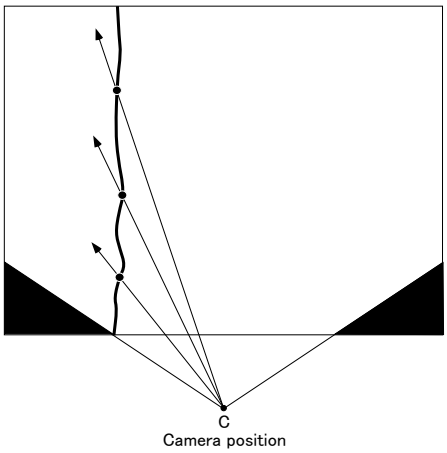

Figure 4: Projection of vertical edges.

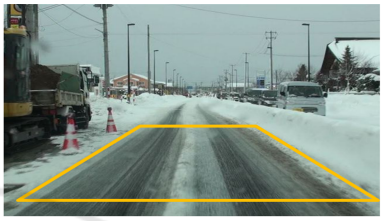

(a) Input image

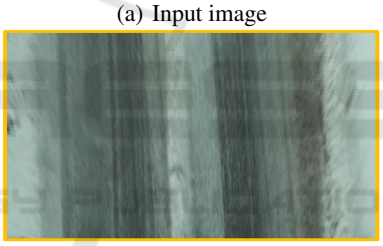

(b) IPM image

Figure 5: Inverse perspective mapping.

4 CREATION OF IPM EDGE IMAGE

In the smooth snow surface, both a road side and a road surface contain only weak texture in the IPM image, as shown in Fig. 6(b). To emphasize slant edges around a road side, the IPM edge image $E_{AND}(u,v)$ is created by the below preprocessing.

1. The vertical edge image $E_v(x,y)$ (Fig. 6(c)) is created by applying the Sobel operator to the input image $I(x,y)$ (Fig. 6(a)). (x,y) is the coordinate value of an image.
2. $E_v(x,y)$ is converted to the IPM image $E_v^{ipm}(u,v)$ (Fig. 6(d)). (u,v) is the coordinate value of the

IPM image.

3. The slant edge image $E_s^{ipm}(u,v)$ (Fig. 6(e)) is created by applying the Sobel operator to the IPM image of $I(x,y)$ (Fig. 6(b)).
4. The AND image $E_{AND}(u,v)$ of $E_v^{ipm}(u,v)$ and $E_s^{ipm}(u,v)$ is created as the preprocessing image for road boundary detection. Figure 6(f) shows $E_{AND}(u,v)$ obtained from $E_v^{ipm}(u,v)$ and $E_s^{ipm}(u,v)$.

Vertical edges on a roadside object are converted into slant edges in the IPM image. On the other hand, there are not many vertical edges on the road surface converted into slant edges. Therefore, in $E_{AND}(u,v)$, slant edges around a road side remains but slant edges on a road surface are suppressed.

5 THE DEGREE OF ROAD BOUNDARY

The vertical edge on the road side object is projected as a shape falling backward radially around the camera position, as shown in Fig.4. Therefore, in each pixel of the IPM edge image, a parallelogram shaped mask is set along a straight line L_{cp} connecting the camera position C and each pixel P, as shown in Fig.7. When parameters V_x, V_y, RX, RY and y_{lim} for creating the IPM image are fixed, the straight line L_{cp} can be determined in advance. An enlarged view of a parallelogram shaped mask is shown in Fig.8. Let the length of the left and right sides of a mask be H, the width between the left and right sides be W, the region on the left side of the point P be R_W and the region on the right side of the point P be R_B.

The road boundary is located on the left side of the IPM image since vehicles drive on the left side of the road in Japan. Since slant edges usually appear densely on road side objects in the IPM edge image, the number of edges in R_W is large and the number of edges in R_B is small if the pixel P is around the road boundary. For this reason, at each pixel P on the left half of the IPM edge image, the degree of road boundary BD is calculated by

$$BD = \frac{(N_W + (S_B - N_B)}{S_W + S_B}, \qquad (2)$$

where N_W is the number of edges in R_W, N_B is the number of edges in R_B , S_w is the total number of pixels of R_w and S_N is the total number of pixels of R_N. The degree of road boundary BD increases around the road boundary since it shows large value when N_W is large and N_B is small.

(a) Smooth snow surface

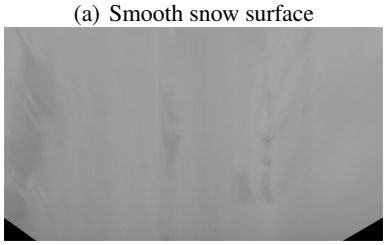

(b) IPM image

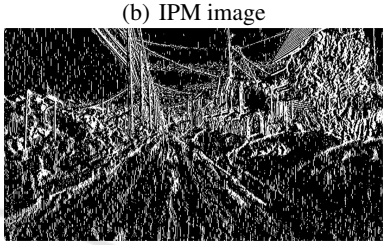

(c) $E_v(x,y)$

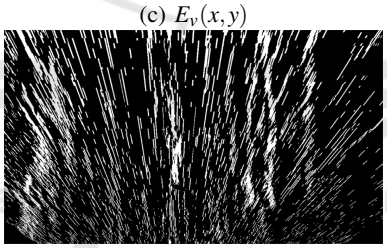

(d) $E_v^{ipm}(u,v)$

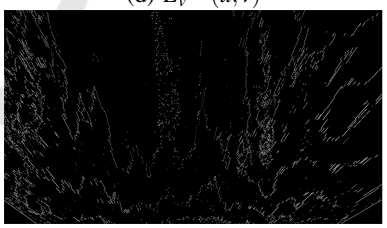

(e) $E_s^{ipm}(u,v)$

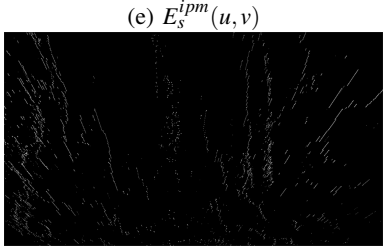

(f) $E_{AND}(u,v)$

Figure 6: Road boundary in smooth snow surface.

Since the camera position C is determined by straight lines k_1k_2 and k_3k_4 indicating the bottom of the IPM image as shown in Fig. 7, the slope θ of the

straight line L_{cp} connecting the camera position C and each pixel P can be calculated in advance. Therefore, our method speeds up the calculation of N_W and N_B by creating the table describing the information of parallelogram shaped mask at each point P. At each pixel P, the same W and H are used for the parallelogram mask. The search angle around C is $\theta_1 < \theta < \theta_2$ and the degree θ is quantized in an integer value. Since the parallelogram in the digital image is approximated like a step as shown in Fig. 9, the shape of the parallelogram mask generated by the parameter (W,H,θ) is limited to several patterns $T_k(k = 0,\ldots,n-1)$. The number of patterns n is uniquely determined when W,H,θ_1 and θ_2 are fixed.

At the pixel $t_i(u_i,v_i)(i = 0,1,\ldots,w-1)$ on the upper side of each pattern T_k, a relative coordinate value $(u_i - u, v_i - v)$ with the center $P(u,v)$ of the mask is calculated. Then, the table $PT_u(k,i)(0 \leq k < n, 0 \leq i < W-1)$ in which $u_i - u$ is stored and the table $PT_v(k,i)(0 \leq k < n, 0 \leq i < W-1)$ in which $v_i - v$ is stored are created for parallelogram shaped mask.

At each pixel $P(u,v)$ of the IPM edge image in the range of $\theta_1 < \theta < \theta_2$, the slope θ of the straight line L_{cp} is calculated in advance, and the index k of the pattern T_k corresponding to the angle θ is written to two-dimensional array $IA(u,v)$ whose size is same as the IPM edge image. θ_1 and θ_2 are determined by manually selecting the upper end A_{max} and the lower end A_{min} of the shoulder in the IPM image which is created from a vehicle parked on the shoulder (Fig.7).

In order to count the number of edges at high speed, the line integral image $S(u,v)(0 \leq u < W_{IPM}, 0 \leq v < H_{IPM})$ in the vertical direction is created by applying the equation (3) to the IPM edge image $E_{AND}(u,v)(0 \leq u < W_{IPM}, 0 \leq v < H_{IPM})$.

$$S(u,v) = \sum_{i=0}^{v} E_{AND}(u,i) \tag{3}$$

Using the line integral image $S(u,v)$, the number of edges E_{num} on the vertical line between the red pixel $t_i(u_i,v_i)$ and the green pixel $e_i(u_i,u_i+H)$ in Fig. 9 is calculated by the equation (4).

$$E_{num} = S(u_i,v_i+H) - S(u_i,v_i) \tag{4}$$

Therefore, at each pixel $P(u,v)$ of the IPM edge image, N_W and N_B in the equation (2) are given by equations 5 and 6 when $IA(u,v)$ is equal to k.

$$N_W = \sum_{i=0}^{\frac{W}{2}-1} (S(u+PT_u(k,i), v+PT_v(k,i)+H) - S(u+PT_u(k,i), v+PT_v(k,i))) \tag{5}$$

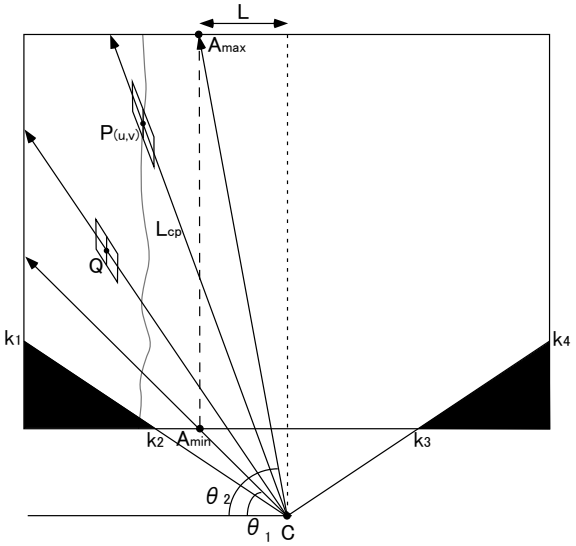

Figure 7: The degree of road boundary.

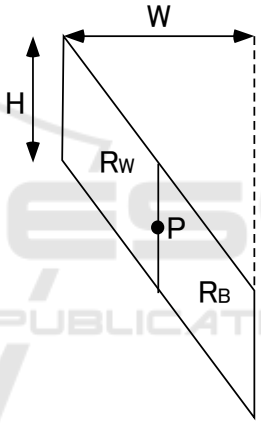

Figure 8: Parallelogram shaped mask.

$$N_B = \sum_{i=\frac{W}{2}}^{W-1} (S(u+PT_u(k,i), v+PT_v(k,i)+H) - S(u+PT_u(k,i), v+PT_v(k,i))) \tag{6}$$

Since both S_W and S_B are $\frac{WH}{2}$, the degree of road boundary BD is calculated from equations (2), (5) and (6). Figure 10(b) shows the example of the degree of road boundary BD calculated from the IPM edge image shown in Fig. 10(a). In this image, an BD is quantized in the range from 0 and 255, and high intensity shows high degree of road boundary.

6 ROAD BOUNDARY TRACKING

Our method detects and tracks the road boundary by Snakes(M. Kass, A. Witkin and D. Terzopoulos,

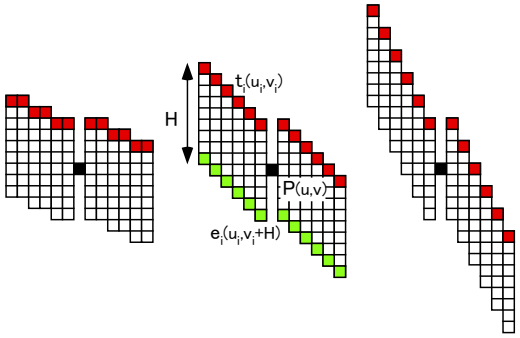

Figure 9: Parallelogram shaped mask in digital image.

1988) whose image force is the degree of road boundary *BD*. First, in the BD image such as Fig. 10(b), the intensity is accumulated vertically and the vertical line passing through the peak is used as the initial position of the Snakes as shown in Fig. 11(a). The number of control points is 61 and the number of updates is 10 per frame. Figure 11(b) shows the convergence result of the Snakes.

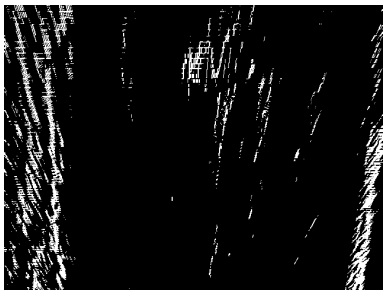

(a) IPM edge image

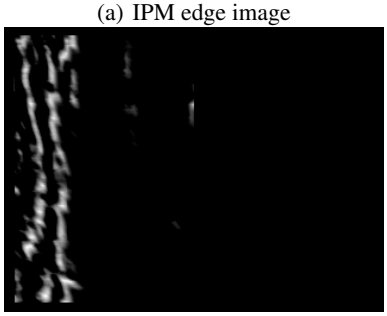

(b) The degree of road boundary

Figure 10: Example of the degree of road boundary.

7 EXPERIMENTS

We conducted experiments to detect the road boundary from images taken by an in-vehicle monocular camera. The KITTI dataset(KITTI,) and our own dataset including snow road scenes were used for qualitative and quantitative evaluation.

7.1 Qualitative Evaluation

Figure 12 show some experimental results using the KITTI dataset. Since Japanese roads are on the right side, we detected the road boundary in the mirror image. In each figure, the left is the detection result overlaid on the input image with a magenta line and the right is the ground truth of the road surface shown in KITTI dataset. In Fig. 12(a), the curb is detected as the road boundary correctly. In Fig. 12(c), the boundary between the road surface and the roadside grass is detected correctly. In Fig. 12(e), The boundary with the parked vehicle is correctly detected.

Since snow road scene is not included in the KITTI dataset, we built the dataset containing various roads covered with snow. We call this dataset HRB(Hirosaki Road Boundary) dataset. Figure 13 shows some experimental results using HRBD. In each figure, the left is the detection result and the right is the ground truth set manually in the IPM image. The HRB dataset also contains road boundaries such as the curb, the roadside grass and so on other than snowy road. In Fig. 13(a) and (c), the curb

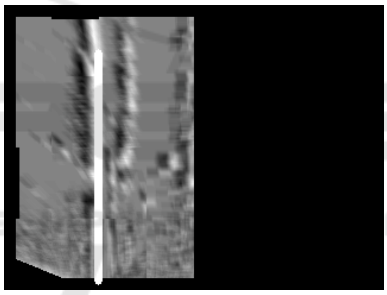

(a) Initial position of Snakes

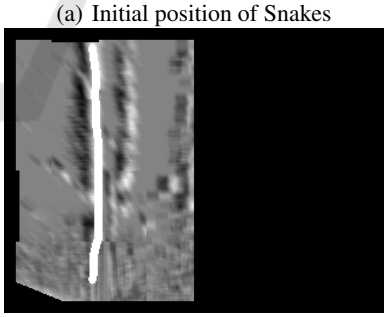

(b) Convergence result

Figure 11: Tracking result of road boundary.

and the roadside grass are detected correctly. Figure 13(e) shows the result in a sherbet-like snow surface, Fig. 13(g) shows the result in a smooth snow surface and Fig. 13(i) shows the result in the scene where the road surface is not covered with snow but a lane marker is occluded by the snow side wall. Although lane markers are invisible in these scenes, the boundary between the snow side wall and a road surface is

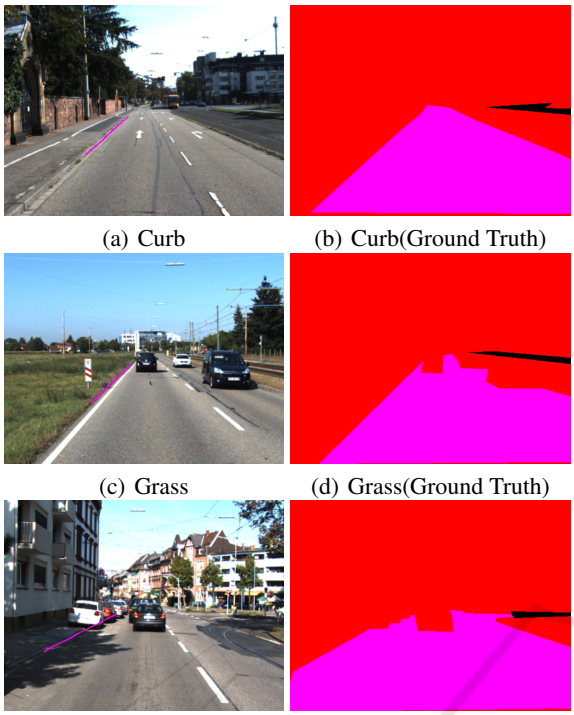

(a) Curb (b) Curb(Ground Truth)

(c) Grass (d) Grass(Ground Truth)

(e) Parked vehicle (f) Parked vehicle(Ground Truth)

Figure 12: Results of road boundary detection (KITTI dataset).

detected correctly as a boundary of the driving lane.

7.2 Quantitative Evaluation

We evaluated the performance of the proposed method quantitatively in the KITTI dataset and the HRB dataset.

In the KITTI dataset, images containing road side objects such as curbs, grasses, vehicles and so on were used for evaluation. 127 frames of the curb and 56 frames of the other road side object including parked vehicles were evaluated. Only the left side of the driving lane in the mirror image was compared with the ground truth tracing the left boundary of the true road area shown in the KITTI dataset.

The HRB dataset contains 100 frames of the curb, 161 frames of the road side grass and 142 frames of the snow side wall. The ground truth was obtained by tracing the road boundary manually in the IPM image.

The detection accuracy DA given by the equation (7) is estimated in the IPM image. Therefore, the ground truth for the KITTI dataset is projected onto the IPM image.

$$DA = \frac{\sum_{i=0}^{n-1} \frac{|p_u(i) - pt_{ux}(i)|}{LaneWidth}}{n} \quad (7)$$

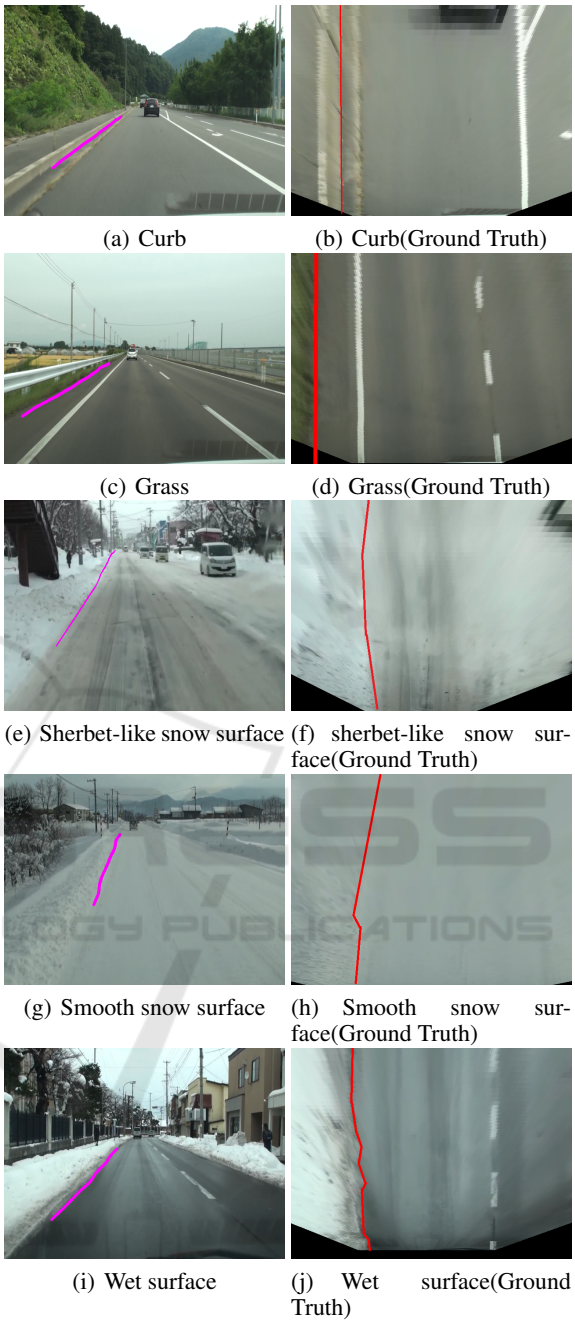

(a) Curb (b) Curb(Ground Truth)

(c) Grass (d) Grass(Ground Truth)

(e) Sherbet-like snow surface (f) sherbet-like snow surface(Ground Truth)

(g) Smooth snow surface (h) Smooth snow surface(Ground Truth)

(i) Wet surface (j) Wet surface(Ground Truth)

Figure 13: Results of road boundary detection (HRB dataset).

Where $p_u(i)$ is the u coordinate value of the control point calculated by the snakes, $pt_u(i)$ is the u coordinate value of the ground truth whose v coordinate value is same as $p_u(i)$, n is the number of the control points in the Snakes and $LaneWidth$ is the width of the driving lane in the IPM image.

Table 1 shows the detection accuracy DA in the KITTI dataset. The average DA of all scenes is 0.088.

Table 1: Detection accuracy (KITTI dataset.)

	# of frames	*DA*
Curb	127	0.095
Other	56	0.071
Total	183	0.088

Table 2: Detection accuracy (HRB dataset.)

	# of frames	*DA*
Curb	100	0.046
Grass	161	0.118
Snow side wall	142	0.080
Total	403	0.087

This result shows that the error of $0.27m$ occurs when the width of the driving lane is about $3m$. However, this result shows that a vehicle has some space to run in the driving lane if the vehicle width is less than $2.5m$. Therefore, the proposed method can also be applied to ordinary vehicles.

Table 2 shows the detection accuracy *DA* in the HRB dataset. The average *DA* of all scenes is 0.087 and *DA* of the snow side wall is 0.08. This result shows that the proposed method is effective for road boundary detection on snowy roads.

8 CONCLUSION

This paper proposed the method to detect the shoulder line of a road including the boundary with the snow side wall from an image of an in-vehicle monocular camera. Vertical lines on an object whose height is different from a road surface are projected onto slanting lines when an input image is mapped to a road surface by the inverse perspective mapping. The proposed method detects a road boundary using this characteristic. In the IPM edge image, the degree of road boundary that responds strongly at the boundary with the area where slant edges are dense is calculated by using the parallelogram shaped mask. The road boundary is tracked by the Snakes whose image force is the degree of road boundary. Experimental results using the KITTI dataset and our own dataset including snow scenes show the effectiveness of the proposed method. The future work is to improve the detection accuracy of distant shoulder.

REFERENCES

A. Laddha, M. K. Kocamaz , L. E. N-serment, and M. Hebert (2016). Map-supervised road detection. In *Proceedings of IV2016*.

B. Hillel, R. Lerner, D. Levi, and G. Raz (2014). Recent progress in road and lane detection: A survey. *Machine Vision and Applications*, 25(3):727–745.

C. Brust, S. Sickert, M. Simon, E. Rodner and J. Denzler (2015). Convolutional patch networks with spatial prior for road detection and urban scene understansing. In *Proceedings of VISAPP2015*.

C. Guo, J. Meguro, Y. Kojima and T. Naito (2013). Cadas: a multimodal advanced driver assistance system for normal urban streets based on road context understanding. In *Proceedings of IV2013*, pages 228–235.

C. Kreucher and S. Lakshmanan (1999). Lana: A lane extraction algorithm that uses frequency domain features. *IEEE Trans. on Robotics and Automation*, 15(2):343–350.

D. Costea and S. Nedevschi (2017). Traffic scene segmentation based on boosting over multimodal low, intermediate and high order multi-range channel features. In *Proceedings of IV2017*.

D. Hoiem, A. A. Efros and M. Hebert (2007). Recovering surface layout from an image. *International Journal of Computer Vision*, 75(1):151–172.

D. Levi, N. Garnett and E. Fetaya (2015). Stixelnet: A depp convolutional network for obstacle detection and road segmentation. In *Proceedings of BMVC2015*.

D. Pfeiffer and U. Franke (2010). Efficient representation of traffic scenes by means of dynamic stixels. In *Proceedings of IV2010*, pages 217–224.

G. L. Oliveira, W. Burgard and T. Brox (2016). Efficient deep models for monocular road segmentation. In *Proceedings of IROS2016*, pages 586–595.

G. Thomas, N. Jerome and S. Laurent (2010). Frequency filtering and connected components charaterization for zebra-crossing and hatched markings detection. In *Proceedings of ISPRS Commision III Symposium*, pages 43–47.

J. C. McCall and M. M. Trivedi (2006). Video-based lane estimation and tracking for driver assistance: Survey, system, and evaluation. *IEEE Trans. on Intelligent Transportation Systems*, 7(1):20–37.

J. K. Suhr and H. G. Jung (2013). Noise resilient road surface and free space estimation using dense stereo. In *Proceedings of IV2013*, pages 461–466.

J. M. Alvarez, T. Gevers and A. M. Lopez (2010). 3d scene priors for road detection. In *Proceedings of CVPR2010*.

J. M. Alvarez, T. Gevers, Y. LeCum and A. M. Lopez (2012). Road scene segmentation from a single image. In *Proceedings of ECCV2012*, pages 376–389.

J. M. Alvarez, Y. LeCum, T. Gevers and A. M. Lopez (2012). Semantic road segmentation via multi-scale ensembles of learned features. In *Proceedings of ECCV2012*, pages 586–595.

J. Siegemund, D. Pfeiffer, U. Franke and W. Forstner (2010). Curb reconstruction using conditional random fields. In *Proceedings of IV2010*, pages 203–210.

J. Zhang and H. Nagel (1994). Texture-based segmentation of road images. In *Proceedings of IV1994*.

J.Douret, R. Labayrade, J. Laneurit and R. Chapuis (2005). A reliable and robust lane detection system based on

the parallel use of three algorithms for driving safety assistance. In *Proceedings of IAPR Conference on Machine Vision Applications*, pages 398–401.

KITTI. The KITTI Vision Benchmark Suite. http://www.cvlibs.net/datasets/kitti/index.php.

M. A. Turk, D. G. Morgenthaler, K. D. Gremban and M. Marra (1988). Vita-a vision system for autonomous land vehicle navigation. *IEEE Trans. on Pattern Analysis and Machine Intelligence*, 10(3).

M. Bertozzi, A. Broggi, M. Cellario, A. Fascioli, P. Lombardi and M. Porta (2002). Artificial vision in road vehicles. *Proceedings of the IEEE*, 90(7):1258–1271.

M. Bertozzi and A. Broggi (1998). Gold: A parallel real-time stereo vision system for generic obstacle and lane detection. *IEEE Trans. on Image Processing*, 7(1):62–81.

M. Enzweiler, P. Greiner, C. Knoppel and U. Franke (2013). Towards multi- cue urban curb recognition. In *Proceedings of IV2013*, pages 902–907.

M. Kass, A. Witkin and D. Terzopoulos (1988). Snakes: Active contour models. *International Journal of Computer Vision*, 1(4):321–331.

M. Meuter, S. Muller-Schneiders, A. Mika, S. Hold, C. Numm and A. Kummert (2009). A novel approach to lane detection and tracking. In *Proceedings of ITSC2009*, pages 582–587.

N. Einecke and J. Eggert (2013). Stereo image warping for improved depth estimation of road surfaces. In *Proceedings of IV2013*, pages 189–194.

R. Mohan (2014). Deep deconvolutional networks for scene parsing. In *ArXiv.org*.

S. Hold, S. Gormer, A. Kummert, M. Meuter, S. Muller-Schneiders (2010). Ela - an exit lane assistant for adaptive cruise control and navigation systems. In *Proceedings of ITSC2010*, pages 629–634.

T. Yasuda and K. Onoguchi (2012). Lane estimation based on lane marking recognition. In *Proceedings of ITS World Congress 2012*.

Z. W. Kim (2008). Robust lane detection and tracking in challenging scenarios. *IEEE Trans. on Intelligent Transportation Systems*, 9(1):16–26.